ISSN 1063-7834, Physics of the Solid State, 2016, Vol. 58, No. 1, pp. 170–176. © Pleiades Publishing, Ltd., 2016.
Original Russian Text © V.S. Gorelik, A.Yu. Pyatyshev, A.S. Krylov, 2016, published in Fizika Tverdogo Tela, 2016, Vol. 58, No. 1, pp. 163–169.

OPTICAL PROPERTIES

Raman Scattering in Sodium Nitrite Crystals near the Phase Transition

V. S. Gorelik[a, *], A. Yu. Pyatyshev[b], and A. S. Krylov[c]

[a] *Lebedev Physical Institute, Russian Academy of Sciences, Leninskii pr. 53, Moscow, 119991 Russia*
[b] *Bauman Moscow State Technical University, Vtoraya Baumanskaya ul. 5, Moscow, 107005 Russia*
[c] *Kirensky Institute of Physics, Siberian Branch, Russian Academy of Sciences, Akademgorodok 50, Krasnoyarsk, 660036 Russia*
**e-mail: gorelik@sci.lebedev.ru*

Received June 22, 2015

Abstract—Optical Raman spectra of a ferroelectric sodium nitrite crystal have been detected in a wide spectrum range at various temperatures, including the region of the ferroelectric phase transition. A manifestation of a transverse soft polar mode of the $A_1(z)$ type responsible for the ferroelectric phase transition has been discovered in the spectrum at room temperature. This mode has been found to become overdamped even far from the ferroelectric phase transition temperature. This mode also appears as a central peak under heating. It has been found that the pseudoscalar mode of the A_2 type has the highest intensity in the Raman spectrum of sodium nitrite. The frequency corresponding to the maximum intensity of this mode in the Raman spectrum varies from 130 cm^{-1} at 123 K to 106 cm^{-1} at $T = 513$ K. A fair agreement of the experimental data for the $A_1(z)$ mode with the Lyddane–Sachs–Teller relation has been established. The polariton curves for the $A_1(z)$ polar mode and the dispersion curves for axinons has been plotted.

DOI: 10.1134/S1063783416010133

Ferroelectric crystals ($BaTiO_3$, KH_2PO_4, $(NH_4)_2BeF_4$, etc.) are widely used in electric and electro-optical devises (capacitors, modulators and memory units [1, 2]). Sodium nitrite ($NaNO_2$) is one of structurally simplest ferroelectric crystals among a great number of substances of this class. $NaNO_2$ crystals undergo a ferroelectric phase transition from a noncentrosymmetric to cetrosymmetric phase at a temperature of 160°C [3]. At room temperature, sodium nitrite that appears in the ferroelectric phase is characterized by space group $C_{2v}^{20}(Im2m)$. As was found, the structure of a sodium nitrite crystal above the Curie temperature corresponds to the space group D_{2h}^{25} (*Immm*). The parameters of the unit cell at temperatures of 26 and 205°C are, respectively: $a = 0.539$ nm, $b = 0.558$ nm, and $c = 0.357$ nm and $a = 0.533$ nm, $b = 0.568$ nm, and $c = 0.369$ nm [4–6]. Voinov et al. [7] and Zaytsev and Yurchenko [8] reported on the experimental results of studying the generation of the second optical harmonic localized in a thin surface layer of globular photonic crystals with sodium nitrite embedded in the pores of the crystals. Zil'berman and Savintsev [9] analyzed the radiation in the megahertz range that appears in sodium nitrite at phase transitions.

The theory [5, 6, 10] predicts that an increase in the dc dielectric function near the ferroelectric phase transition point is caused by the presence of a so-called soft mode in the vibrational spectrum—a transverse polar (TO) oscillation classified by a full-symmetry irreducible representation (A_1) in the pyroelectric phase.

Infrared spectra of a $NaNO_2$ crystal were studied in many works [11–16]. Therein, the reflection spectra were detected in the frequency region of 40–600 cm^{-1} in the temperature range from 293 to 503 K. The reflection spectra were analyzed in [11–13]. The A_1 (TO) mode responsible for the dielectric anomaly at the phase transition point at 433 K was found to appear in the vibrational spectrum of sodium nitrite.

The analysis of the Raman spectra of sodium nitrite crystals was a subject of many works [17–23]. In these works, the effect of temperature (in the range of 300–500 K) on the Raman spectrum was investigated [17, 18]. In [19], the Raman spectra of a single crystal at temperatures of 77 and 294 K were studied and the detected spectral bands were associated with the oscillation types. The soft polar mode of the A_1(TO) type responsible for the ferroelectric phase transition has not been so far revealed in the Raman spectra of sodium nitrite.

In this work, we aimed at analyzing a complete Raman spectrum of a sodium nitrite crystal at various

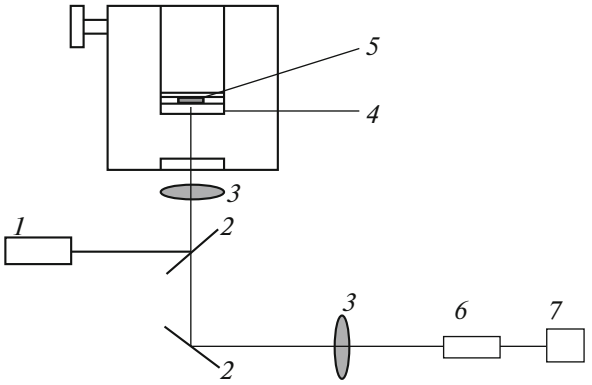

Fig. 1. Scheme of the experimental setup with the (*1*) laser, (*2*) mirror, (*3*) lens, (*4*) glass substrate, (*5*) sample, (*6*) T64000 triple monochromator, and (*7*) computer.

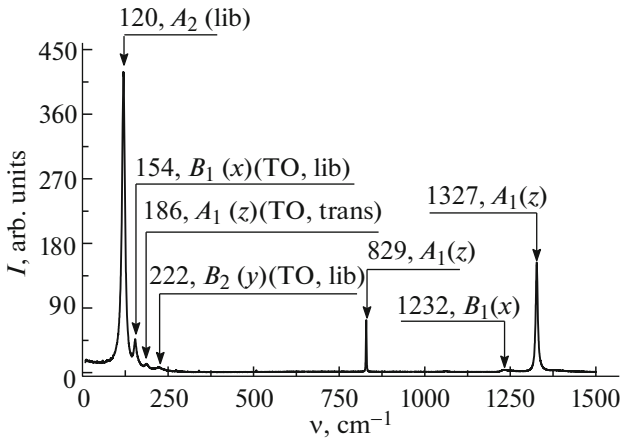

Fig. 2. Complete Raman spectrum of sodium nitrite detected at room temperature in the frequency range from 0 to 1500 cm^{-1}.

temperatures and revealing of the soft mode of the A_1(TO) type in the spectrum, as predicted by the theory for ferroelectric crystals. In addition, we aimed to study the temperature dependence of the pseudoscalar mode of the A_2 type corresponding to the libration oscillations of the NO_2 group with respect to the polar axis of the crystal.

The principal scheme of the experimental setup for the excitation and detection of Raman spectra is shown in Fig. 1. A 15-mW Spectra Physics Stabilite 2017 argon laser (*1*) with a wavelength of 514.5 nm was used as the excition radiation source. The laser beam after passing a turn mirror (*2*) was focused by an objective (*3*) on a sample (*5*). We used a 50-fold microlens ($f = 0.8$ mm) with a numerical aperture of 0.75. A powder sodium nitrite sample under investigation was squeezed between a transparent glass (*4*) and a liquid nitrogen vessel.

The scattered light was detected with the use of a mirror (*2*) and a lens (*3*). The Raman spectra were detected with the use of a Horiba Jobin Yvon T64000 triple monochromator (*6*). The detector was a CCD matrix, the signal from which was transmitted to a computer (*7*). The spectral resolution was 1 cm^{-1}, the diffraction gratings with 1800 lines/mm were used, the width of the input slit was 0.1 mm.

Figure 2 shows the complete Raman spectrum (in the region of lattice and intramolecular modes) of polycrystalline sodium nitrite detected at room temperature in the frequency range from 0 to 1500 cm^{-1}. As is seen, the spectrum consists of a region corresponding to lattice modes and the region corresponding to intramolecular oscillations.

Figures 3a and 3b illustrate the Raman spectrum in the region of lattice modes of a sodium nitrite crystal at room temperature and at 123 K in the frequency range of 0–300 cm^{-1}. Figure 3a presents the spectral region corresponding to lattice modes at room temperature. Arrows indicate the positions of the respec-

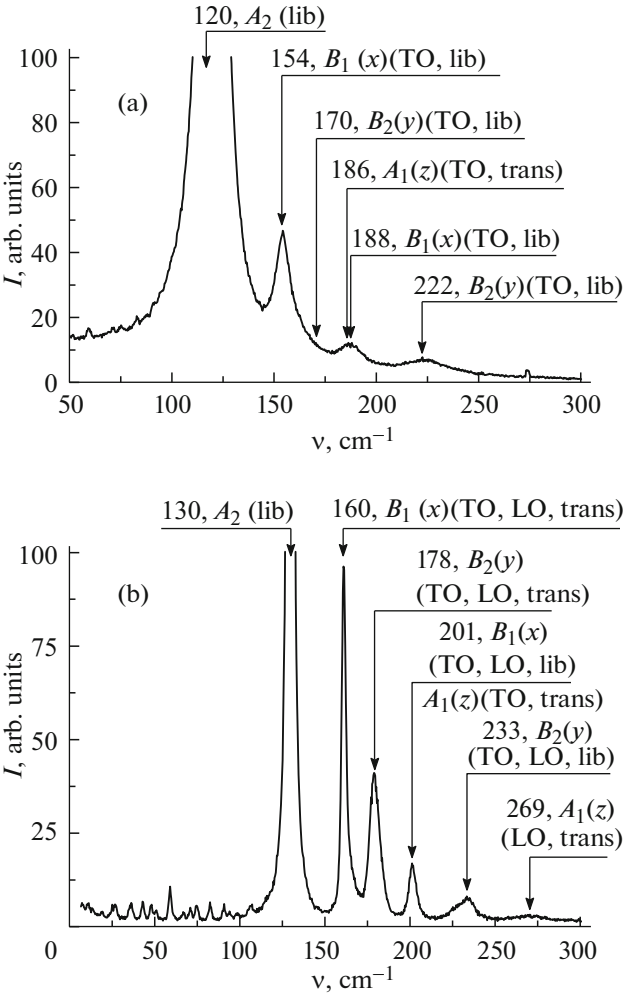

Fig. 3. Low-frequency part of the Raman spectrum of sodium nitrite (a) at room temperature and (b) at T = 123 K.

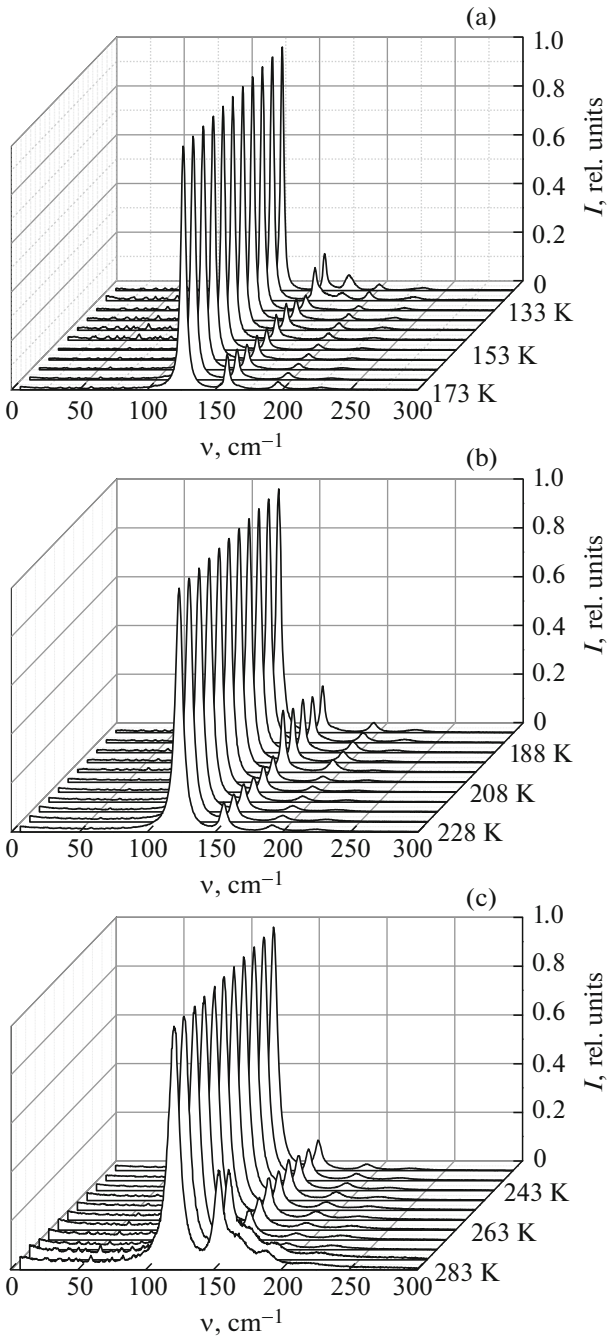

Fig. 4. Evolution of the low-frequency Raman spectra at temperatures of (a) 123–173, (b) 178–228, and (c) 223–283 K.

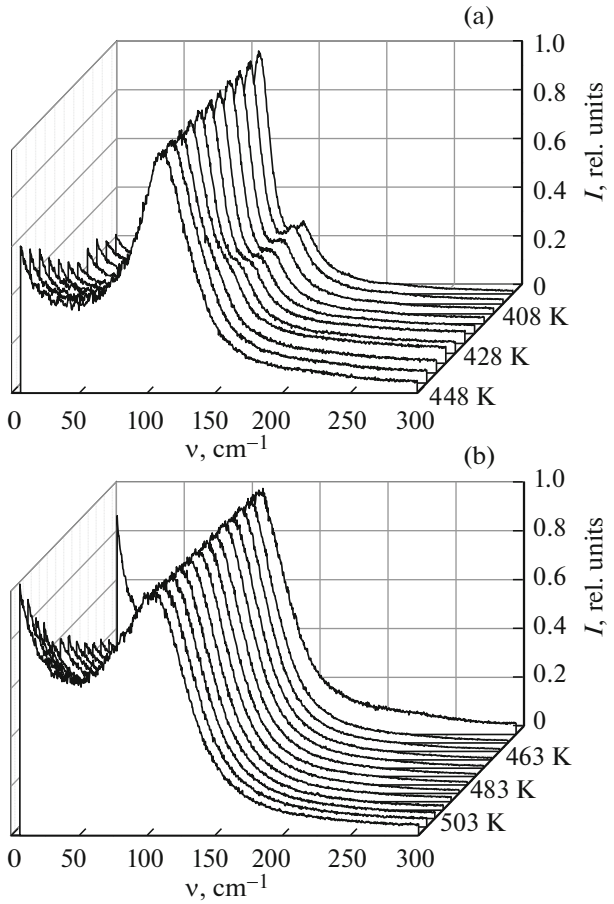

Fig. 5. Temperature dependence of the low-frequency Raman spectra near the ferroelectric phase transition temperature at (a) 398–448 and (b) 453–513 K.

tive intensity maxima; the frequency values, the symmetry types and assignment in terms of the (trans) translational or (lib) librational character of the modes are also quoted. As is seen in Fig. 3a, a weak band appears at room temperature at a frequency of 186 cm^{-1}, which is close to the data of infrared spectroscopy (194 cm^{-1}) [11, 12], corresponding to the A_1(TO) type, a soft mode responsible for the ferroelectric transition.

The Raman satellites in the region of lattice modes become narrower with a decrease in temperature (Fig. 3b) than at room temperature (Fig. 3a). The Raman spectrum contains a peak at a frequency of 130 cm^{-1} (a pseudoscalar mode of the A_2 type), the intensity of which is considerably higher than the intensities of other lattice modes. There is also a Raman line with a maximum at a frequency of 201 cm^{-1}. The presence of this satellite agrees with the data [11, 12] on the IR spectra of sodium nitrite, in the soft mode of the A_1(TO) type was revealed at room temperature at a frequency of 194 cm^{-1}.

Figures 4a–4c illustrate the variation of the low-frequency Raman spectra of sodium nitrite in the temperature range of 123–283 K.

As is seen in Fig. 4, the line, whose frequency varies within 120–130 cm^{-1} with a decrease in temperature from 283 to 123 K, is most intense in the low-frequency Raman spectra. In addition, the low-frequency Raman spectra include weak bands in the region of 150–200 cm^{-1}, the intensity of which are redistributed with a decrease in temperature.

Table 1. Literature data on the infrared reflection spectra and Raman spectra of sodium nitrite

	IR, cm^{-1}				Raman, cm^{-1}						Character
	[11]		[12]		[17]		[18]		[22, 23]		
	TO	LO	TO	LO	TO	LO	TO	LO	TO	LO	
$A_1(z)$	194	269	187	–	–	–	–	–	–	–	Translational
$B_1(x)$	157	163	151	–	153	–	154	165	158	–	
$B_2(y)$	149	193	146	–	–	–	150	201	–	–	
A_2	–		–		119		120		117		Librational
$B_1(x)$	188	250	181	–	177	–	184.5	236	191	–	
$B_2(y)$	223	261	232	–	220	–	228	254	223	–	
$A_1(z)$	826	829	825	–	825	–	828	829	830	–	Internal
$A_1(z)$	1323	1336	1321	–	1327	–	1326	1328	1323	–	
$B_1(x)$	1235	1368	1227	–	1280	–	1225	1356	1230	–	

The variation of the low-temperature Raman spectrum in the region of the ferroelectric phase transition with an increase in temperature (T_C = 436 K) is illustrated in Figs. 5a and 5b.

As the temperature approaches the ferroelectric phase transition (T = 433 K), a low-frequency wing appears, the intensity of which increases monotonically (Fig. 5a, the temperature range of 398–448 K). The intensity of the low-frequency wing exhibits a sharp increase a 453 K (Fig. 5b, the curve at T = 453 K). With a further increase in temperature (T > 460 K), the intensity of the low-frequency wing first decreases and then increases (Fig. 5b, curves at T = 458–513 K).

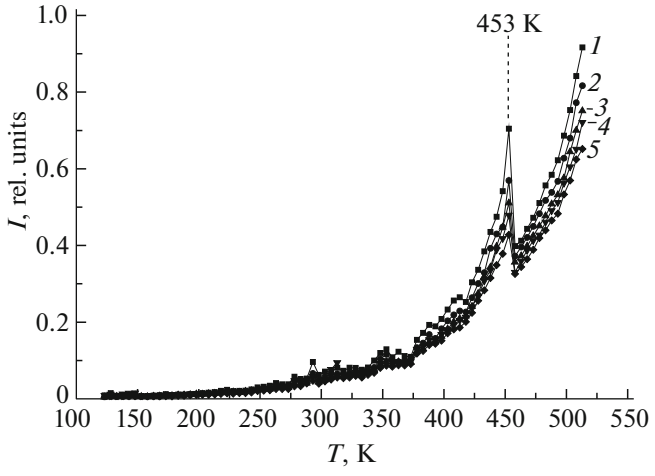

Fig. 6. Fixed-frequency temperature dependence of the intensity the lines at (*1*) 10, (*2*) 15, (*3*) 20 (*4*) 25, and (*5*) 30 cm^{-1}.

As is seen in Figs. 5a and 5b, the low-frequency mode A_2 in the Raman spectrum broadens and is shifted toward lower frequencies from 120 to 105 cm^{-1} with an increase in temperature from 293 to 513 K. This mode does not exhibit any significant changes in the Raman spectrum in the region of the ferroelectric phase transition (T = 433 K). All other modes appear as diffuse, overlapping weak bands upon heating of the crystal. Figure 6 present fixed-frequency temperature dependences of the intensity of Raman scattering at frequencies of 10, 15, 20, 25, and 30 cm^{-1}. To produce these dependences, we used the numerical data on the Raman spectra measured at various temperatures and fixed frequencies.

As is seen in Fig. 6, as well as in Fig. 5b (the curve at T = 453 K), there is an intensity maximum at T = 453 K at all fixed frequencies (10, 15, 20, 25, and 30 cm^{-1}). As is known [24], there is a sinusoidal (incommensurate) phase of sodium nitrite that appears in a narrow temperature range (436.8–438 K) between the ferroelectric and antiferroelectric phases. In addition, the measurements of the temperature dependence of the specific heat [25] revealed an anomaly corresponding to an antiferroelectric–paraelectric phase transition at T = 453 K. Thus, the observed anomaly in the fixed-frequency temperature dependences of the Raman spectra confirms the presence of the antiferroelectric–paraelectric phase transition of sodium nitrite at a temperature of 453 K.

According to the group-theory analysis of the vibrational spectrum of a sodium nitrite crystal, the spectrum of optical modes of the ferroelectric phase includes the following oscillation types [26]:

$$T_{opt} = [A_1(z) + B_1(x) + B_2(y)] + [A_2 + B_1(x) + B_2(y)] + [A_1(z) + A_1(z) + B_1(x)]. \quad (1)$$

Table 2. Oscillation frequencies and their assignment to the symmetry types in the room-temperature Raman spectrum of sodium nitrite

Frequency, cm^{-1}	Mode symmetry type	Phonon type	Mode type	Character
186	$A_1(z)$	TO	Translational	Lattice
154	$B_1(x)$	TO		
170	$B_2(y)$	TO		
120	A_2		Librational	
188	$B_1(x)$	TO		
222	$B_2(y)$	TO		
829	$A_1(z)$	LO	Symmetric bending mode	Internal
1327	$A_1(z)$	TO	Symmetric stretching mode	
1232	$B_1(z)$	TO	Asymmetric stretching mode	

The first square bracket corresponds to translational (trans) lattice modes (translational oscillations of the NO_2 group with respect to sodium ions); the second square bracket stands for librations (lib) of the NO_2 group with respect to three axes; the third bracket corresponds to intramolecular (internal) vibrations of the NO_2 group. The polar modes $A_1(z)$, $B_1(x)$, and $B_2(y)$ should appear in the Raman spectra as transverse (TO) and longitudinal (LO) components. Table 1 presents the literature data on the symmetry types and oscillation types found from the analysis of infrared reflection spectra and Raman spectra of sodium nitrite crystals.

Table 2 lists the frequencies of the maxima in the room-temperature Raman spectra of polycrystalline $NaNO_2$ observed in this work. In contrast to the literature data (Table 1), we discovered in the room-temperature Raman spectra (Figs. 2 and 3) a lattice mode of the $A_1(z)$ type with a frequency of 186 cm^{-1} corresponding to the translational transverse polar oscillation of the A_1(TO) type responsible for the ferroelectric phase transition.

The frequencies of the maxima in the low-frequency Raman spectrum of sodium nitrite measured at the temperature $T = 123$ K are given in Table 3.

As follows from comparison of Figs. 2 and 3 and Tables 2 and 3, the frequencies of Raman lines exhibit shifts toward higher values with a decrease in temperature from room temperature to 123 K. There are satellites in Fig. 3b at frequencies of 201 and 269 cm^{-1}, which correspond (according to the data of infrared spectroscopy [11, 12]) to the oscillations of the A_1(TO) and A_1(LO) types. It is worth mentioning that in this case the soft mode corresponding to the $A_1(z)$(TO) mode appears to be overdamped far from the ferroelectric phase transition point. This is caused by reorientations of the NO_2 group around the x axis, which leads to dephasing of the $A_1(z)$(TO) mode. As a result, this mode becomes a relaxer with an increase in temperature and appears as a broadband low-frequency wing typical for relaxation processes. The found values of the characteristics of the soft mode of sodium nitrite far from the ferroelectric phase transition temperature and the respective values of the high-frequency and dc dielectric functions are listed in Table 4.

According to the well-known Lyddane–Sachs–Teller relation [27] for the soft mode $A_1(z)$ responsible for the ferroelectric phase transition, it should be (neglecting the contribution of internal modes)

$$\frac{\varepsilon_{0z}}{\varepsilon_{\infty z}} = \frac{\omega^2_{(\mathrm{LO},A_1(z))}}{\omega^2_{(\mathrm{TO},A_1(z))}}. \quad (2)$$

Substituting the values from Table 4 to Eq. (2) we conclude that the Lyddane–Sachs–Teller relation agrees fairly well with the experimental data on the

Table 3. Oscillation frequencies and their assignment to the symmetry types in the Raman spectrum of sodium nitrite detected at the temperature $T = 123$ K

Frequency, cm^{-1}	Mode symmetry type	Phonon type	Mode type
130	A_2		Librational
160	$B_1(x)$	TO, LO	Translational
178	$B_2(y)$	TO, LO	
201	$B_1(x)$	TO, LO	Librational
233	$B_2(y)$	TO, LO	
269	$A_1(z)$	LO	Translational

Table 4. Parameters of polaritons for the A_1 mode at room temperature

Mode	ν, A_1(TO), cm^{-1}	ν, A_1(LO), cm^{-1}	$\varepsilon_{\infty z}$[11]	ε_{0z} [12]
$A_1(z)$	186	269	1.9	3.51

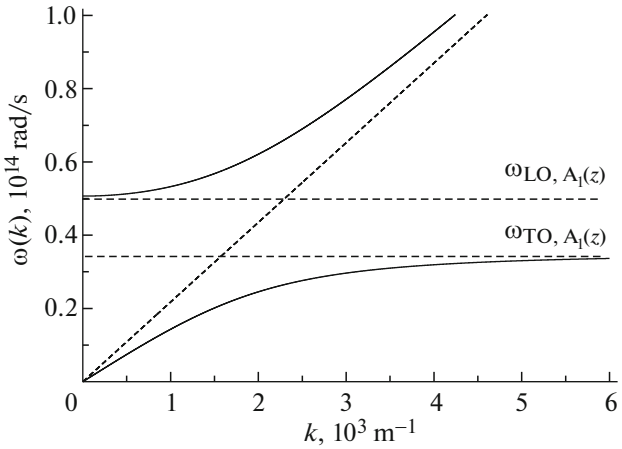

Fig. 7. Polariton curves for the $A_1(z)$ mode at room temperature.

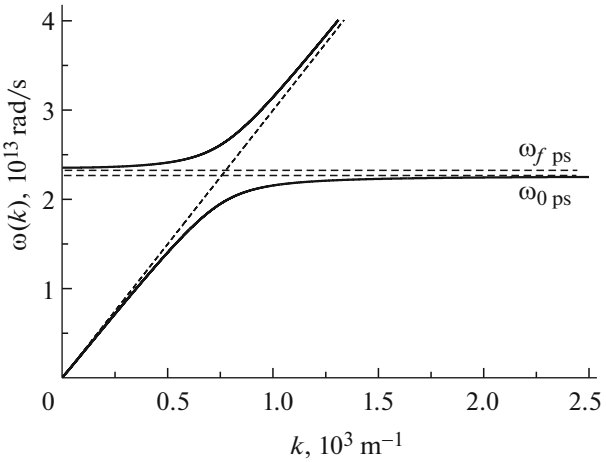

Fig. 8. Dispersion curves of axinon branches in sodium nitrite.

Raman spectra and the literature data of infrared spectroscopy.

Based on the found characteristics of the soft mode, we can build the dispersion relation for the respective polariton curves specified by the known formula

$$\omega^2 = \frac{c_0^2 k^2}{\varepsilon_z(\omega)}. \quad (3)$$

Here, c_0 is the speed of light in vacuum and $\varepsilon_z(\omega)$ is the respective dielectric function

$$\varepsilon_z(\omega) = \varepsilon_{\infty z}\frac{\omega^2_{\mathrm{LO},A_1(z)} - \omega^2}{\omega^2_{\mathrm{TO},A_1(z)} - \omega^2}. \quad (4)$$

Substituting Eq. (4) into Eq. (3) we find the relation for the dispersion curves of polaritons

$$\omega^4 - \omega^2\frac{\omega^2_{\mathrm{LO},A_1(z)}\varepsilon_{\infty z} + c_0^2k^2}{\varepsilon_{\infty z}} + \frac{\omega^2_{\mathrm{TO},A_1(z)}c_0^2k^2}{\varepsilon_{\infty z}} = 0. \quad (5)$$

As a result, we find the solution for two polariton branches

$$\omega^2_{\pm}(k) = \frac{\omega^2_{\mathrm{LO},A_1(z)} + c^2k^2}{2} \times\left(1 \pm \sqrt{1 - \frac{4\omega^2_{\mathrm{LO},A_1(z)}c^2k^2}{(\omega^2_{\mathrm{LO},A_1(z)} + c^2k^2)^2}}\right). \quad (6)$$

Here, $c^2 = \dfrac{c_0^2}{\varepsilon_{\infty z}}$, $\omega_{\mathrm{LO},A_1(z)} = 2\pi c_0\nu(\mathrm{LO}, A_1(z))$, $\omega_{\mathrm{TO},A_1(z)} = 2\pi c_0\nu(\mathrm{TO}, A_1(z))$. The parameters $\nu(\mathrm{LO}, A_1(z))$, $\nu(\mathrm{TO}, A_1(z))$, and $\varepsilon_{\infty z}$ are given in Table 4. Figure 7 shows the results of computing the form of the polariton curves for the polar mode $A_1(z)$ in sodium nitrite. The $\omega_{\mathrm{TO},A_1(z)}$ and $\omega_{\mathrm{LO},A_1(z)}$ values and the dispersion relation $\omega = \dfrac{c_0k}{\sqrt{\varepsilon_{\infty z}}}$ are also shown (by dashed lines).

According to the table of characters of irreducible representations of group C_{2V} [28], the librational lattice modes are classified by the pseudoscalar symmetry type A_2. According to the theoretical concepts elaborated in [29–36], in addition to electromagnetic waves, there exist pseudoscalar waves in vacuum corresponding to elementary particles referred to as axions. The resonance interaction of axions with pseudoscalar phonons in a dielectric medium leads to the formation of hybrid quasiparticles—axinons [37]—similar to polaritons. In [37], the dispersion relation for axinons was found to be

$$\omega^2_{\pm}(k) = \frac{(\omega^2_{f\mathrm{ps}} + \omega_a^2 + c_0^2k^2)}{2} \times\left(1 \pm \sqrt{1 - \frac{4(\omega^2_{0\,\mathrm{ps}}\omega_a^2 + \omega^2_{0\,\mathrm{ps}}c_0^2k^2)}{(\omega^2_{f\mathrm{ps}} + \omega_a^2 + c_0^2k^2)^2}}\right). \quad (7)$$

Here, $\omega_{f\,\mathrm{ps}} = 2\pi c_0\nu_{f\,\mathrm{ps}}$, $\omega_a = 2\pi c_0\nu_a$, and $\omega_{0\,\mathrm{ps}} = 2\pi c_0\nu_{0\,\mathrm{ps}}$. We use the following values of the parameters: $\nu_{f\,\mathrm{ps}} = 125\ \mathrm{cm}^{-1}$, $\nu_{0\,\mathrm{ps}} = 120\ \mathrm{cm}^{-1}$ (Table 2), $\nu_a = 1\ \mathrm{cm}^{-1}$ [38, 39]. Figure 8 shows the dispersion curves of sodium nitrite found with the use of Eq. (7). The dashed lines correspond to the dispersion relation of photons in vacuum and specify the values of the parameters $\omega_{f\,\mathrm{ps}}$ and $\omega_{0\,\mathrm{ps}}$.

As is seen in Fig. 8, the axion branch and the dispersion branch of the pseudoscalar mode of sodium nitrite exhibit anticrossing in the crossover region, which is typical for hybridization of interacting modes.

In conclusion, we have discovered the presence of the transverse polar mode of the $A_1(z)$ type (soft mode) responsible for the ferroelectric phase transi-

tion of sodium nitrite in the Raman spectrum of this crystal. It turned out that this mode is pronounced in the Raman spectrum only far from the ferroelectric phase transition point, at low temperatures of the sample. With an increase in temperature, this mode becomes, overdamped and can appear only as a central peak. Upon approaching to the ferroelectric phase transition point, the central peak is seen as a broad relaxation wing near the exciting line. The intensity of this peak exhibits a sharp maximum at the temperature $T = 453$ K. As a result of the analysis of the low-frequency temperature dependences, we have confirmed the presence of an antiferroelectric–paraelectric phase transition of sodium nitrite at a temperature of 453 K.

The assignment of all the Raman satellites predicted by the group-theory analysis has been carried out. The room-temperature polariton curves for the soft mode $A_1(z)$ have been built. It has been found that the intensity of the pseudoscalar mode A_2 is an order of magnitude greater than the intensities of other lattice modes. The possibility of hybridization of pseudoscalar phonons with axions has been discussed. The found behavior of the polar and pseudoscalar modes in sodium nitrite can be used for the observation of parametric processes accompanied by generation of radiation in the terahertz spectrum range.

ACKNOWLEDGMENTS

This study was supported by the Russian Foundation for Basic Research (project nos. 12-02-00491, 13-02-00449, 13-02-90420, and 14-02-00190).

REFERENCES

1. P. Ravindran, A. Delin, B. Johansson, O. Eriksson, and J. M. Wills, Phys. Rev. B: Condens. Matter **59**, 1776 (1999).
2. J. Köhler and D. Schmid, J. Phys.: Condens. Matter **8**, 115 (1996).
3. B. Strijk and C. H. Mac Gillavry, Recl. Trav. Chim. Pays-Bus. **62**, 705 (1943).
4. R. W. G. Wyckoff, *Crystal Structures*, Vol. 2: *Inorganic Compounds RXn, RnMX2, RnMX3* (Interscience, New York, 1964).
5. F. Jona and G. Shirane, *Ferroelectric Crystals* (Pergamon, Oxford, 1962).
6. G. A. Smolenskii, V. A. Bokov, V. A. Isupov, N. N. Krainik, R. E. Pasynkov, and M. S. Shur, *Ferroelectrics and Antiferroelectrics* (Nauka, Leningrad, 1971) [in Russian].
7. Yu. P. Voinov, V. S. Gorelik, K. I. Zaitsev, L. I. Zlobina, P. P. Sverbil', and S. O. Yurchenko, Phys. Solid State **57** (3), 453 (2015).
8. K. I. Zaytsev and S. O. Yurchenko, Appl. Phys. Lett. **105**, 051902 (2014).
9. P. F. Zil'berman and P. A. Savintsev, Sov. Tech. Phys. Lett. **14** (1), 64 (1988).
10. V. L. Ginzburg, Usp. Fiz. Nauk **38**, 490 (1949).
11. J. D. Axe, Phys. Rev. **167**, 573 (1968).
12. M. K. Barnoski and J. M. Ballantyne, Phys. Rev. **174**, 946 (1968).
13. K. Suzuki, S. Sawada, F. Sugawara, and T. Nakamura, J. Phys. Soc. Jpn. **26**, 1199 (1969).
14. H. Vogt and H. Happ, Phys. Status Solidi B **16**, 711 (1966).
15. F. Brehat and B. Wyncke, J. Phys. C: Solid State Phys. **18**, 1705 (1985).
16. B. Wyncke, F. Brehat, M. El. Sherif, and G. V. Kozlov, Phys. Status Solidi B **125**, 493 (1984).
17. E. V. Chisler and M. S. Shur, Phys. Status Solidi B **17**, 163 (1966).
18. C. M. Hartwig, E. Wiener-Avnear, and S. P. S. Porto, Phys. Rev. B: Solid State **5**, 79 (1972).
19. C. K. Asawa and M. K. Barnoski, Phys. Rev. B: Solid State **2**, 205 (1972).
20. C. W. yon der Lieth and H. H. Eysel, J. Raman Spectrosc. **13**, 120 (1982).
21. H. H. Eysel, C. W. von der Lieth, G. Bertsch, and M. H. Brooker, Mol. Phys. **44**, 395 (1981).
22. M. Tsuboi, M. Terada, and T. Kajiura, Bull. Chem. Soc. Jpn. **41**, 2545 (1968).
23. M. Tsuboi, M. Terada, and T. Kajiura, Bull. Chem. Soc. Jpn. **42**, 1871 (1969).
24. Y. Yamada, I. Shibuya, and S. Hoshino, J. Phys. Soc. Jpn. **18**, 1594 (1963).
25. S. Hoshino, J. Phys. Soc. Jpn. **19**, 140 (1964).
26. G. Ya. Lyubarskii, *The Application of Group Theory in Physics* (GIFML, Moscow, 1958; Pergamon, London, 1960).
27. R. H. Lyddane, R. G. Sachs, and E. Teller, Phys. Rev. **59**, 673 (1941).
28. L. D. Landau and E. M. Lifshitz, *Course of Theoretical Physics*, Vol. 3: *Quantum Mechanics: Non-Relativistic Theory* (Nauka, Moscow, 1989; Butterworth–Heinemann, Oxford, 1991).
29. L. B. Okun', Sov. Phys. JETP **56** (3), 502 (1982).
30. K. van Bibber, N. R. Dagdeviren, S. E. Koonin, A. K. Kerman, and H. N. Nelson, Phys. Rev. Lett. **59**, 759 (1987).
31. L. D. Duffy, P. Sikivie, D. B. Tanner, S. J. Asztalos, C. Hagmann, D. Kinion, L. J. Rosenberg, K. van Bibber, D. B. Yu, and R. F. Bradley, Phys. Rev. D: Part., Fields, Gravitation, Cosmol. **74**, 012006 (2006).
32. P. Sikivie, D. B. Tanner, and K. van Bibber, Phys. Rev. Lett. **98**, 172002 (2007).
33. A. Afanasev, O. K. Baker, K. B. Beard, G. Biallas, J. Boyce, M. Minarni, R. Ramdon, M. Shinn, and P. Slocum, Phys. Rev. Lett. **101**, 120401 (2008).
34. S. Hoffmann, Phys. Lett. B **193**, 117 (1987).
35. R. Cameron, G. Cantatore, A. C. Melissinos, G. Ruoso, Y. Semertzidis, H. J. Halama, D. M. Lazarus, A. G. Prodell, F. Nezrick, C. Rizzo, and E. Zavattini, Phys. Rev. D: Part. Fields **47**, 3707 (1993).
36. G. Ruoso, R. Cameron, G. Cantatore, A. Melissinos, Y. Semertzidis, H. Halama, D. Lazarus, A. Prodell, F. Nezrick, C. Rizzo, and E. Zavattini, Z. Phys. C: Part. Fields **56**, 505 (1991).
37. V. S. Gorelik, Kratk. Soobshch. Fiz. **42**, 40 (2015).
38. C. Beck, Phys. Rev. Lett. 111, 231 801 (2013).
39. C. Hoffmann, F. Lefloch, and M. Sanquer, Phys. Rev. B: Condens. Matter **70**, 180503 (2004).

Translated by A. Safonov